

Buoyancy Effects on Mantle Flow Under Mid-Ocean Ridges

WUSI SU AND W. ROGER BUCK

Lamont-Doherty Earth Observatory and Department of Geological Sciences of Columbia University, Palisades, New York

Results of a series of two-dimensional numerical experiments of mantle flow, melting, and melt migration under a spreading center are reported. The model predicts the distribution of melt in the subridge mantle, the width over which most melt is delivered to the crust, and the thickness of crust. The sources of buoyancy considered are thermal expansion, compositional variation caused by melt extraction, and the phase change of solid to melt. We infer that the steady state average viscosity of the mantle below a ridge cannot be much less than about 10^{19} Pa s. For a lower average viscosity, thermal convection causes rapid cooling of a large region under a ridge, raising the viscosity. Results imply that transient increases in mantle temperature should lead to larger increases in the oceanic crustal thickness for slow spreading ridges than for fast spreading ridges. We assume that the viscosity is proportional to $\exp(-\phi/\phi_0)$, where ϕ is melt fraction. We parameterize the permeability in terms of the reference velocity for percolation of the melt v_r , where the relative velocity of melt to solid is $v_r \phi$. Analytic approximations are used to extrapolate the model results to large values of permeability and small values of ϕ_0 . If v_r is less than 1 m/yr, then more melt would be retained in the subridge mantle than is estimated from analysis of topography and gravity data at fast spreading centers. For v_r greater than about 100 m/yr, so little melt would be retained in the mantle that it is difficult to explain the gravity data and the low shear wave velocity structure close to the East Pacific Rise estimated from seismic surface waves. Buoyancy effects can lead to a region of mantle upwelling and melting that is as narrow as the observed zone of oceanic crustal accretion. For most melt to be added to the crust within a few kilometers of a fast spreading center requires that ϕ_0 be less than 0.015 if v_r equals 1 m/yr and less than 0.003 if v_r is 100 m/yr.

INTRODUCTION

It has long been accepted that oceanic crust is the product of pressure release melting of mantle as it rises under a spreading center. Petrological and isotopic studies indicate that melting begins at a depth greater than 60 km [e.g., *Salters and Hart, 1989*] and that the average degree of partial melting of the mantle is about 10% [*Klein and Langmuir, 1987*]. To explain the average thickness of oceanic crust, which is 6-7 km [*Chen, 1992*](Z. C. Mutter and J. C. Mutter, Variations in thickness of layer 3 dominate oceanic crustal structure, submitted to *Earth and Planetary Science Letters*, 1992; hereinafter referred to as Mutter and Mutter, submitted manuscript, 1992), most of the melt that is produced by the upwelling would have to be removed from the mantle. Topography and seismic observations indicate that the crust attains its full thickness no more than a few kilometers from the neovolcanic zone of fast spreading centers [*Detrick et al., 1987*].

If mantle upwelling at a spreading center is a passive response to plate separation, then significant melting should occur to more than 100 km from a ridge axis for the fastest spreading ridges (see results below). Thus we would expect the crust to thicken continuously far from a ridge, contrary to observations. One way to explain the narrowness of the zone of crustal accretion is if the mantle upwelling is focused into a narrow region below a spreading center. The density of the mantle beneath a ridge may be lower than elsewhere due to the temperature structure, due to the change in composition of the residual mantle when melting occurs, and due to the retention of some amount of melt in the solid matrix. Several authors [e.g., *Rabinowicz et al., 1984; Scott and Stevenson, 1989; Sotin and Parmentier, 1989*] have suggested that the lower density of the mantle near a ridge could drive focused upwelling flow.

Other processes have been suggested to cause melt to concentrate to make crust close to a ridge crest. *Spiegelman and McKenzie [1987]* showed how the nonhydrostatic pressure gradient sustained by corner flow could cause lateral movement of melt toward the ridge axis. They find that to extract melt from a wide area requires a mantle viscosity greater than 10^{21} Pa s. Such large viscosity values at shallow depths in the mantle are not consistent with several geophysical observations (see discussion by *Buck and Parmentier [1986]*). *Phipps Morgan [1987]* proposed that the finite strain due to corner flow could cause anisotropic permeability, in turn causing lateral movement of melt. This model requires that as melting begins an isotropic distribution of veins exists which is deformed by the mantle flow. *Sparks and Parmentier [1991]* suggested that dilatation of the porous matrix creates a high-porosity boundary layer beneath an impermeable cap of cooler, solid mantle. The along-layer component of gravity drives melt in this highly permeable layer toward the ridge axis. Though these processes may contribute to focusing melt into a narrow zone, we do not consider them in our model calculations.

Existing data do not uniquely constrain which processes control the narrowness of the zone of crustal accretion. Geochemical data from mid-ocean ridge basalts suggest that melt migration occurs in a state of at least partial chemical disequilibrium [*Klein and Langmuir, 1987; McKenzie and Bickle, 1988*]. This is consistent with small melt fractions being transported from the middle of the melting region to the surface on a time scale of a few thousand years. Data on highly incompatible trace elements are interpreted to require efficient removal of melt fractions as small as 0.1% from the mantle [*Plank and Langmuir, 1992*]. Geophysical data require that more melt is retained in the mantle below ridges than geochemical data appear to permit. Shear wave velocity-depth profiles derived from surface wave studies of the East Pacific Rise (EPR) show lower velocities in the top 50 km of the mantle within the youngest age zones of the rise axis than farther away [*Forsyth, 1992*]. The velocity contrast is

Copyright 1993 by the American Geophysical Union.

Paper number 93JB00994.
0148-0227/93/93JB-00994\$05.00

consistent with the presence of more than 2% melt in the mantle close to the ridge. Topography and gravity data for the EPR at 9°-14°N, 6°-11°S and 16°-21°S appear to require that the subridge mantle be at least 1% lower in density than mantle elsewhere [Madsen *et al.*, 1984; Wilson, 1992]. A similar analysis of data for the EPR between 7° and 9°S requires such a density contrast to extend to approximately 20 km depth below the seafloor (X. Wang and J. R. Cochran, Gravity anomalies, isostasy, and mantle flow at the East Pacific Rise crest, submitted to *Journal of Geophysical Research*, 1992; hereinafter referred to as Wang and Cochran, submitted manuscript, 1992). Such a density contrast is consistent with the presence of several percent melt below the ridge.

There is also no clear picture of how melt should segregate from the mantle on the basis of laboratory experiments. It has long been held that melt in an olivine matrix should reside completely on grain triple junctions [Waff and Bulau, 1979]. Analysis of new experiments and reanalysis of old experiments indicate that significant melt may reside on grain faces [Waff and Faul, 1992]. This should reduce the permeability of the mantle to melt flow compared to flow along triple junctions. There is also controversy over how much effect melt will have on reducing the viscosity of an aggregate partial melt [e.g., Cooper and Kohlstedt, 1984; Borch and Green, 1990].

Because the constraints on state of partial melting under ridges are not strong, it is meaningful to test a range of different cases through theoretical models. These calculations can show which material parameters affect possible observable quantities such as the distribution of melt below the spreading center. These results may aid in the design of experiments to test general models.

This paper has two goals. The first is to demonstrate the effects of different sources of density variations on the pattern of mantle upwelling under a spreading center. For example, temperature variations have a very different effect on the flow pattern than do variations in the amount of melt retained in the mantle. We also examine how the dependence of viscosity on temperature and on melt fraction retained in the mantle can affect the pattern of upwelling and melting. The second goal of the paper is to identify the range of parameters that could lead to subridge mantle upwelling that is narrow enough to explain the observed width of the zone of crustal accretion.

The most important and uncertain parameters in our model are the permeability of the mantle and the relation between viscosity and melt fraction. In our previous work [Buck and Su, 1989] we were interested in showing the effect of melt dependent mantle viscosity on the focusing of upwelling under a ridge. We considered an extremely small value of permeability for melt migration. In this paper we consider the widest range of permeabilities that we can model numerically and go on to develop a simple analytic model which allows us to predict the amount of focusing for a wider range of permeabilities.

MODEL FORMULATION

The modeling of mantle flow and melting is based on the following assumptions. As mantle is pulled upward by the separation of lithosphere plates it undergoes pressure release melting. Melt and matrix move laterally together. The vertical movement of the melt relative to the matrix is described by Darcy's law. Density variations are caused by thermal expansion, the change in composition of the residual caused by

extraction of melt, and retention of low-density melt within the mantle matrix. Energy changes due to latent heat and frictional heating between matrix and melt are ignored. Including the latent heat term would lower temperatures with height above the base of the melting region. However, the melting temperature of the mantle also changes with depth, and the combined effect of this and the cooling due to the latent heat of fusion is not well known. The viscosity may depend only on temperature or on temperature and melt fraction.

Governing Equations

The stream function of a two-dimensional incompressible flow satisfies a biharmonic equation with a source term

$$\nabla^2(\mu\nabla^2\psi) = -g\frac{\partial\rho}{\partial x} + 2 * \left[\frac{\partial^2\mu\partial^2\psi}{\partial x^2\partial z^2} + \frac{\partial^2\mu}{\partial z^2}\frac{\partial^2\psi}{\partial x^2} - 2 * \frac{\partial^2\mu}{\partial x\partial z}\frac{\partial^2\psi}{\partial x\partial z} \right], \quad (1)$$

where ρ is density, g is the acceleration due to gravity, μ is viscosity of matrix with melt, and x and z are the horizontal and vertical coordinates. The meanings of all parameters in equations of this paper can be found in Table 1. As usual, the horizontal and vertical components of velocity V of mean motion of solid matrix and melt are $\partial\psi/\partial z$ and $-\partial\psi/\partial x$, respectively. The relationship between the velocities of liquid V_m , solid V_s , and mean motion are [Scott and Stevenson, 1989]

$$V = \phi V_m + (1-\phi)V_s, \quad (2)$$

where ϕ is the porosity or melt fraction.

The distribution of the temperature field is controlled by conservation of energy

$$\frac{\partial T}{\partial t} = -V \cdot \nabla T + \kappa \nabla^2 T, \quad (3)$$

where κ is the thermal diffusivity and T is the potential temperature (i.e., the temperature with an adiabatic temperature gradient removed). We assume that mantle enters the box with temperature T_m .

The distributions of composition and porosity are controlled by [Scott and Stevenson, 1989]

$$\frac{\partial\phi}{\partial t} = -V_s \cdot \nabla\phi - (1-\phi)\nabla[\phi(V_m - V_s)] - R_0\frac{\partial\psi}{\partial x} \quad (4)$$

and

$$\frac{\partial F}{\partial t} = -V_s \cdot \nabla F - R_0\frac{\partial\psi}{\partial x}, \quad (5)$$

where F represents the degree of melting and

$$R_0 = \frac{\partial F_m}{\partial T} * \frac{\partial T}{\partial z} + \frac{\partial F_m}{\partial p} * \frac{\partial p}{\partial z} \quad (6)$$

is the rate of melting due to decompression on ascent in the melting region and is equal to zero below it. F_m is the melting function defined below. Note that we assume that $R_0(-\partial\psi/\partial x)$ cannot be less than zero, so this term is always a source and freezing in our calculations is ignored. Both ϕ and F can be affected by advection, and porosity can also be changed by

TABLE 1. Parameters Used in Equations (1)-(12)

Variable	Meaning	Value Used	Dimension
ψ	stream function of matrix		$\text{m}^2 \text{s}^{-1}$
μ	local shear viscosity of mantle		Pa s
g	acceleration due to gravity	9.81	m s^{-2}
ρ	local density		kg m^{-3}
$V_m, V_s,$ and V	velocities of melt, solid, and mean motion (vectors)		m s^{-1}
ϕ	melt fraction		none
T	temperature		$^{\circ}\text{C}$
K	thermal diffusivity of lithosphere	10^{-6}	$\text{m}^2 \text{s}^{-1}$
R_0	rate of melting due to decompression		m^{-1}
F	depletion		none
ρ_0	density at $T = T_m$ and $F = \phi = 0$	3300	kg m^{-3}
T_m	mantle temperature	1300	$^{\circ}\text{C}$
α	coefficient of thermal expansion	$3 \cdot 10^{-5}$	$^{\circ}\text{C}^{-1}$
β	coefficient of density variation caused by depletion	0.05	none
γ	coefficient of density variation caused by melt fraction	0.152	none
μ_0	reference viscosity of mantle	$10^{18} - 10^{20}$	Pa s
ϕ_0	characteristic porosity controlling the dependence of viscosity on melt fraction	0.01-0.033	none
E	activation energy	420	kJ mol^{-1}
R	universal gas constant	8.3144	$\text{J mol}^{-1} \text{ } ^{\circ}\text{C}^{-1}$
F_m	melting function		none
p	pressure		MPa
$k\phi$	permeability at porosity at ϕ		m^2
a	grain size	$10^{-4} - 10^{-2}$	m
b	constant in permeability	3000	none
ρ_m	density of melt	2800	kg m^{-3}
μ_m	shear viscosity of melt	10	Pa s
V_r	reference percolation velocity = $v_r z$		m s^{-1}
v_p	plate velocity	1.0-7.5	cm/yr

melt migration. Equations (4) and (5) reflect conservation of physical quantities ϕ and F themselves. However, the effects on conservation of momentum and energy caused by variations of ϕ and F are not considered in our pseudo-two-phase model.

State Equations

The density is considered to depend on temperature T , the degree of depletion F , and the melt fraction ϕ presented in a local area of the mantle as

$$\rho = \rho_0 [1 - \alpha (T - T_m) - \beta F - \gamma \phi]; \quad (7)$$

where ρ_0 is the density at $T = T_m$ and $F = \phi = 0$ and is 3300 kg/m^3 . The reference temperature $T_m = 1300^{\circ}\text{C}$. The values of the constants are given as $\alpha = 3 \times 10^{-5} \text{ } ^{\circ}\text{C}^{-1}$, $\beta = 0.05$, and $\gamma = 0.152$ [Scott and Stevenson, 1989]. The value of γ is determined by the difference in density between melt and solid. Here $\gamma = (\rho_0 - \rho_m) / \rho_0$ where ρ_m is the density of melt ($= 2800 \text{ kg/m}^3$). For those values a 100°C change in temperature produces the same change in density as a depletion of 6% or the retention of 2% melt as shown in Figure 1.

It is widely accepted that viscosity is an exponential function of inverse temperature [Weertman and Weertman, 1975], but the dependence of viscosity on melt fraction is debatable. Cooper and Kohlstedt [1986] suggest that the presence of several percent melt in an ultramafic partial melt causes viscosity to be reduced by a factor between 2 and 5. However,

recent results of Borch and Green [1990] suggest that much larger reductions in viscosity are possible at relatively low melt fractions. We will consider the effect of both weak and strong dependences of viscosity on melt fraction. To do this, we assume an exponential relation between them. Thus the complete viscosity function we use is

$$\mu(T) = \mu_0 \exp [(E/R)(1/T - 1/T_m)] \exp (-\phi/\phi_0). \quad (8)$$

The viscosity is μ_0 when $T = T_m$ and $\phi = 0$. The variables in our calculations are μ_0 and ϕ_0 . For $\phi_0 = 1\%$ the viscosity is reduced by a factor of 10 for $\phi = 2.3\%$. The activation energy E determines the temperature dependence of viscosity and is a well-determined quantity for olivine. For the value of E equal to 420 kJ/mol the viscosity goes up by a factor of 10 for every 100°C drop in temperature. We have neglected any pressure dependence of viscosity in the interest of simplicity since any increase in viscosity with depth should have little effect on the flow pattern close to a ridge.

The melting function F_m is assumed to follow a simple linear relation with temperature and pressure above the solidus [McKenzie, 1984; Sotin and Parmentier, 1989]

$$F_m(T, p) = (T - T_0) / 600.0 = (T - 1180 - 0.06p) / 600.0, \quad (9)$$

where T is in degrees Celsius and p is in megapascals. It gives the degree of melting at a place where an initially solid material is brought to given pressure p and temperature T . If material is

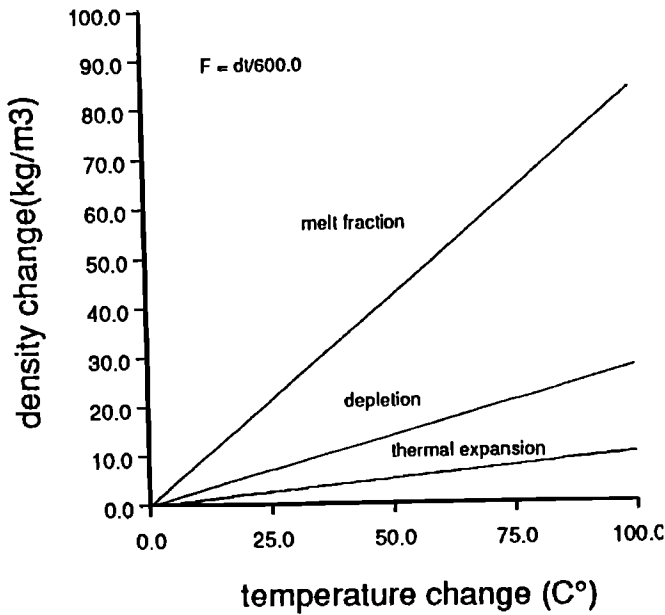


Fig. 1. Buoyancy effects due to thermal expansion, depletion, and melt retention as temperature increases by 100°C.

brought up from depth and melted to 10% and subsequently cooled or advected downward, the degree of depletion F will remain at its maximum value of 10% even though the value of F_m is less than that.

Experiments have shown that basaltic melt in equilibrium with olivine can form a mostly interconnected network of channels along intergranular edge intersections [Waff and Bulau, 1979]. For melt to segregate from the solid matrix it must overcome the resistance to flow through such a network of channels and the matrix must be able to compact as melt is removed. Spiegelman [1993a, b] discusses the importance of the viscous resistance of the matrix to compaction and shows that this term controls the flow of melt near obstructions in the melt flux and causes melt extraction to be strongly time-dependent. However, for steady state problems where there are no rapid variations in the melt flux, viscous resistance to

compaction can be neglected [Ahern and Turcotte, 1979; Ribe, 1985; Spiegelman, 1993a, b]. Here we will treat the segregation of melt in terms of flow through a porous medium where the measure of resistance to flow is the permeability. Assuming that all melt is located along edge intersections, a relationship between porosity (or melt fraction) and permeability k_ϕ will have the form

$$k_\phi = (a^2/b) * \phi^2, \tag{10}$$

where a is the grain size and b is a constant which has been estimated to be about 3000 for ultramafic partial melts [Cheddle, 1989]. Since basaltic melt is less dense than the ultramafic residuum, it will be driven to flow vertically due to a pressure gradient of $(\rho_0 - \rho_s)g$. If the difference in vertical velocity of melt relative to solid is governed by Darcy's law, it will be given by

$$V_m - V_s = k_\phi (\rho_m - \rho_0) g / (\phi \mu_m) \hat{z}, \tag{11}$$

where g is the acceleration of gravity, μ_m is the melt viscosity, here taken to be 10 Pa s [Kushiro, 1986]. We introduce v_r the reference percolation velocity for Darcy flow as follows

$$v_r = (V_m - V_s) / \phi = a^2/b (\rho_m - \rho_0) g / \mu_m \hat{z} = v_r \hat{z}. \tag{12}$$

The reference percolation velocity times the porosity gives the velocity of melt relative to the solid matrix. Taking $a = 1$ mm makes v_r equal 5.25 m/yr, and for $\phi = 0.01$ (1%) the melt would flow at 0.0525 m/yr.

Boundary Conditions

We consider a model box filled with viscous fluid representing an area of the mantle including a spreading center (Figure 2). A typical box is 200 km deep and extends 200 km laterally from the ridge axis. The right side of the box is a symmetry boundary representing a vertical surface passing through a ridge crest. At this boundary there is no lateral flow of material and heat. The surface is made to move horizontally at a constant velocity except close to the ridge crest where the velocity cosine tapers to zero over a distance of 5 km. The

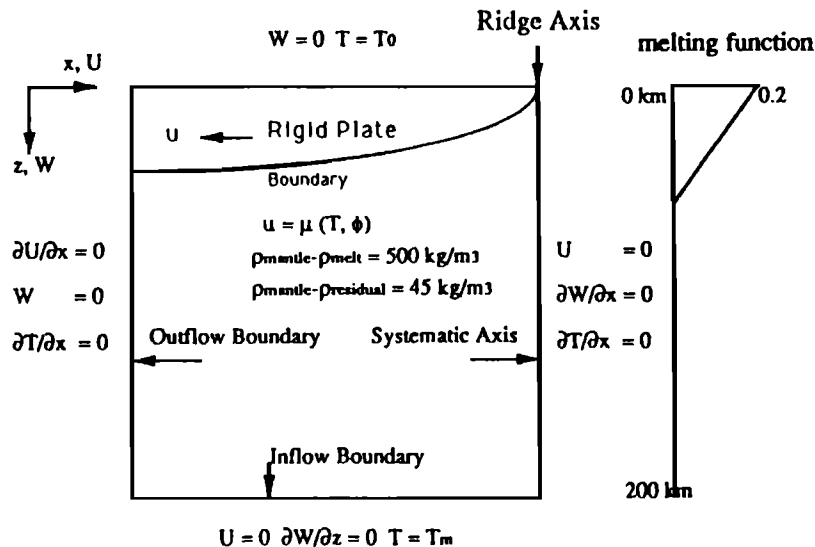


Fig. 2. Boundary conditions for flow and temperature fields, and melting function.

temperature at the surface is kept at 0°C. Regions colder than 1050°C are assumed frozen and specified to move as a rigid plate. Material can pass through the left and bottom boundaries where the viscous normal stress and the vorticity are specified to be zero. The temperature T_m of the material which goes into the box from below is fixed to 1300°C, and at the left side there is no lateral conduction of heat.

In order to resolve the details of flow and melting under a ridge we must limit the size of the numerical box considered. We cannot solve the above equations for the flow in the whole mantle. Other workers [e.g., *Scott and Stevenson, 1989; Sotin and Parmentier, 1989*] have used fixed velocity boundary conditions at the bottom of the box and at the side where material leaves the box. We have let the flow field determine how fast material enters and leaves the box. Neither our boundary condition nor the fixed velocity conditions are entirely correct, but they can be considered as extremes of a range of possibilities. Fixing boundary velocities assumes that buoyancy effects do not change the flow field outside of the box. For our boundary conditions, buoyancy effects can lead to more material flowing through the model box, but the temperature of the material flowing into the box is not affected by the buoyancy-driven flow. As long as buoyancy effects are localized in the subaxial region, and the boundaries are far from that region, then the material going through the boundaries is driven only by the motion of the spreading plates. If buoyancy effects extend to the edges of the box, then extra flow can be driven through the boundaries.

The above equations and boundary conditions can only be solved numerically. A finite difference technique for an irregularly spaced grid is employed [*Parmentier, 1975*]. This allows a fine mesh in the region of rapidly varying viscosity without an inordinately large number of grid points overall. The spatial derivatives in equations (1), (3), (4), and (5) are approximated using three-point central differences. The advective terms of equations (3), (4), and (5) are approximated by the upwind form discussed by *Torrance [1968]*. The time derivative is given by the forward difference. The time step is restricted to ensure stability of the temperature equation following *Lax and Richtmyer [1956]*. Their definition of stability is that the numerical solution converges to the exact solution of the differential equations as grid spacing approaches zero. Expressions (4) and (5) are two-dimensional nonlinear hyperbolic equations. It is difficult to discuss the stability and artificial diffusion of two-dimensional nonlinear differential equations in general. However, after simplifying the problem to one dimension, *Scott and Stevenson [1989]* discussed the conditions of the stability of the flow and pointed that when the ratio of half spreading rate to reference percolation velocity is reduced to a critical value, the behavior of the flow becomes episodic and nonstable in their model. This is consistent with our calculations. After linearizing, artificial diffusion of equations (4) and (5) can be discussed like thermal convection. We started a group of calculations by running the code at a coarse grid spacing for the most difficult case of that group in terms of low viscosity or high permeability. We decreased the grid size until further reduction made a negligible difference to the solutions. This grid is then used for the rest of the calculations in this group. A smaller time step is used to obtain stable solutions and to avoid artificial diffusion to equations (4) and (5) than is used for advancing the energy equation. In our calculations a grid spacing of 0.5-1.0 km was used in the region of most rapid

flow. Gradually, the grid spacing increases to about 5 km far from the ridge. At least 100 points were used in each direction.

RESULTS

Flow Patterns at Ridges for Different Cases

The mantle flow pattern is controlled by viscous forces created by plate separation and buoyancy related to several kinds of density variations. Viscous stresses are controlled by the viscosity of mantle material which should be a function of both temperature and melt fraction in the matrix (see equation (8)). Density variations may be a consequence of thermal expansion, the compositional changes due to depletion of the matrix, and the retention of melt in mantle matrix (see equation (7)). Since there are so many factors which can affect the flow pattern, we begin with the simple case of flow driven by plate separation alone, with the viscosity of the mantle only a function of temperature. Next we add the buoyancy caused by thermal expansion. After that, the effect of compositional variations due to depletion of the matrix is included. Up to this point, the only uncertain variable is the average viscosity of the mantle. The last density effect is the retention of melt, and this depends on a very poorly known relation between porosity (fraction of volume occupied by melt) and permeability. In the final case the effective matrix viscosity is assumed to depend on the melt fraction present. The relationship between μ and ϕ is also not well known.

Figure 3 shows the streamlines for a number of calculations all with the same full spreading rate of 0.10 m/yr and melting rate. The stream functions here and in Figures 6 and 10 are shown with contours that are equally spaced between the maximum and minimum values on the grids. The reference viscosity constant $\mu_0 (=10^{18}$ Pa s) is also the same for all cases as is E , the activation energy per mole ($=420$ kJ/mol). Only in Figure 3e do we show the effect of viscosity depending on melt fraction. Figures 3a-3d differ only in how the density is treated. These differences are as follows.

In Figure 3a the density is constant so that the mantle flow is driven solely by the separation of the plates. The strong dependence of viscosity on temperature causes the upwelling to be slightly more focused under the spreading center than it is for simple corner flow [see *Batchelor, 1967*]. In Figures 3a-3c we calculate where melting is occurring and assume that melt instantly migrates vertically to add to the crust. For flow driven by plate separation, significant melting occurs 50 km from the ridge for this spreading rate.

In Figure 3b we add the effect of thermal buoyancy. The flow then becomes slightly more concentrated under the ridge. Because lateral density gradients drive flow toward the ridge (see equation (1)), the focusing in Figure 3b is caused by the gradient of temperature close to the ridge crest. As we discuss below, the effects of thermal buoyancy can extend beyond the local area of the subridge mantle melting and have significant effects besides the slight concentration of upwelling.

The next effect we add is the density change due to depletion, and results are illustrated by Figure 3c. The flow becomes even more concentrated under the ridge, and the crust attains 90% of its thickness within about 25 km of the spreading center. The upwelling is narrower for the same reason that the inclusion of thermal buoyancy affected the flow pattern. When the temperature is above the solidus for fertile mantle, any variations in temperature will have a big effect on the degree of melting, through equation (9), and hence on the density of the

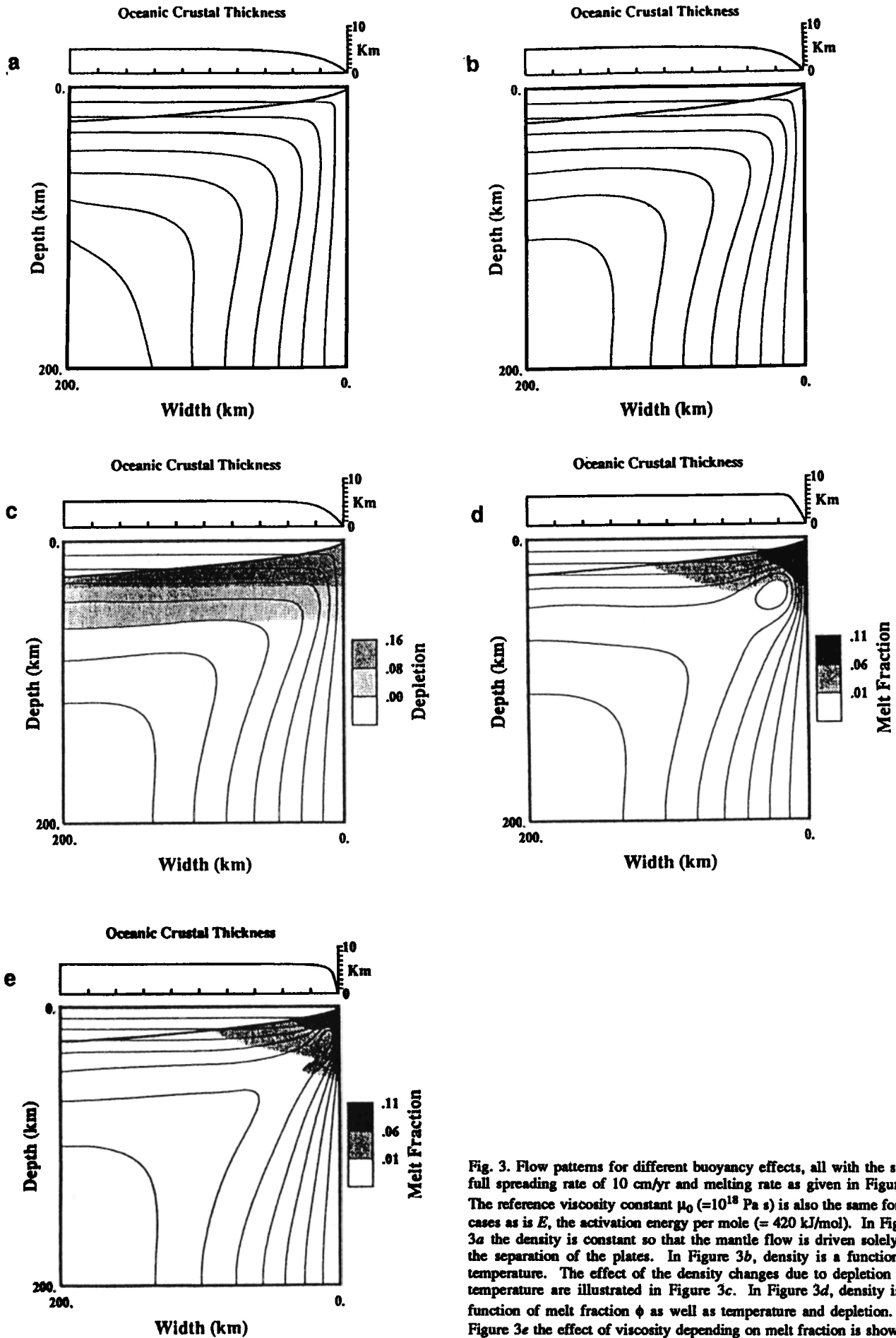


Fig. 3. Flow patterns for different buoyancy effects, all with the same full spreading rate of 10 cm/yr and melting rate as given in Figure 2. The reference viscosity constant μ_0 ($=10^{18}$ Pa s) is also the same for all cases as is E , the activation energy per mole ($=420$ kJ/mol). In Figure 3a the density is constant so that the mantle flow is driven solely by the separation of the plates. In Figure 3b, density is a function of temperature. The effect of the density changes due to depletion and temperature are illustrated in Figure 3c. In Figure 3d, density is a function of melt fraction ϕ as well as temperature and depletion. In Figure 3e the effect of viscosity depending on melt fraction is shown.

residuum. Variations in temperature above the solidus affect the density more because of the change in the residual composition than because of thermal expansion (see Figure 1). As long as material is upwelling and melting, the thermal expansion effect and the depletion effect act to cause the same sign of density variation near a ridge. Lateral temperature variations under a spreading center will cause the mantle to be more depleted and hence lighter under the ridge than at the same depth away from the center of upwelling.

Away from the area of upwelling the density changes due to depletion and thermal expansion do not act in concert. If it is too cold at a given position for further melting, depletion can be changed only by advection, while temperatures are changed by advection and conduction. Also, the density structure produced by depletion is stably stratified, with light mantle on top of denser (less depleted) mantle. The thermal structure away from the upwelling zone is potentially unstable since cold, high-density material is perched above hot, lower-density mantle. These effects will be discussed further below.

In Figure 3d, density is a function of melt fraction ϕ as well as temperature and depletion. In this calculation we assume that the reference percolation velocity for Darcy flow v_r is 0.50 m/yr. This corresponds to assuming an average grain size of about 0.3 mm in calculating the permeability via equation (10). In later calculations we consider the effect of assuming larger grain sizes and so larger values of v_r . As shown in Figure 3d the buoyancy effect of melt retention causes more focusing of upwelling under the ridge. This occurs because more melt is retained in the area of rapid upwelling than in the adjacent areas.

We calculate the crustal thickness assuming that all melt delivered to the base of the lithosphere efficiently segregates by vertical flow from the mantle to form the crust. The lithosphere extends to the depth where the temperature is less than 1050°C. Note that in Figure 3d the region of most crustal growth is within 10 km of the spreading center. This is significantly narrower than for the case shown in Figure 3c which neglected the effect of melt buoyancy and had a wider zone of upwelling.

In Figure 3e the viscosity is not only a function of temperature but also of melt fraction. For this case we choose ϕ_0 in equation (8) equal to 0.033. Comparing Figure 3e with Figure 3d, we see that upwelling is concentrated into a narrower region and the depth where the flow changes from vertical to horizontal under the spreading center takes place at a much shallower depth. It is easy to understand why this tight focusing occurs. In the region where the melt fraction is large the viscosity is reduced. The lower viscosity allows upwelling to occur faster in a narrower region. More melt is retained in a faster upwelling and so the viscosity is further reduced. Eventually, an equilibrium width of upwelling is established.

The shallow depth where the streamlines of mantle flow turn from horizontal to vertical may be important to the pattern of crustal accretion. The flow can change directions in a short distance because the shallow subridge mantle viscosity is low for Figure 3e. For this case the viscosity is reduced by more than a factor of 10 where ϕ is greater than 8%. The melt produced in the narrow upwelling is advected nearly to the base of the crust. Therefore less melt is carried laterally away from the ridge with the flowing mantle.

From Figure 3a to Figure 3e we added different buoyancy terms and the effect of melt fraction dependent viscosity. All these factors speed up the upwelling under ridges. Since more mantle reaches a shallow depth before cooling, the focusing of

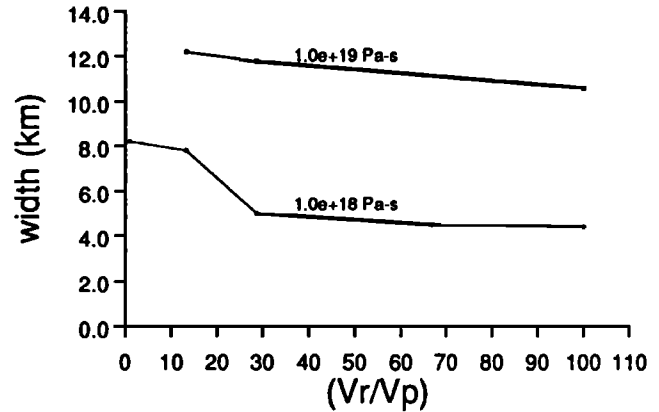


Fig. 4. Relationship between the width for crustal accretion and the ratio of v_r (Darcy velocity, see equation (12)) to v_p (half spreading rate). The vertical axis shows the width of the region where half of the melt reaches the crust. The parameter on the horizontal axis is related to the assumed permeability. For the calculations with a viscosity of 10^{19} Pa s there is little effect of the buoyant flow on width of the region of crustal accretion. With $\mu_0 = 10^{18}$ Pa s the crustal accretion zone is narrowest for v_r/v_p between about 30 and 100.

upwelling under a ridge causes more material to melt and makes the crust thicker. Note that the different upwelling patterns have little effect on the position of the isotherm defining the lithosphere.

In the remaining calculations described in this paper the density is taken to depend on temperature, depletion, and melt fraction according to equation (7) with $\alpha = 3 \times 10^{-5} \text{C}^{-1}$, $\beta = 0.05$, and $\gamma = 0.152$. We vary only the reference viscosity μ_0 , reference percolation velocity v_r , and the parameter controlling the viscosity dependence on melt fraction ϕ_0 .

Effect of Varying Mantle Permeability, Spreading Rate, and Reference Viscosity

The effect of changes in the assumed permeability, as expressed by the reference percolation velocity, on the width of the zone of crustal accretion is shown in Figure 4. The vertical axis shows the distance from the center of spreading to the point where the thickness of the crust reaches half of the maximum thickness. The parameter on the horizontal axis is the ratio of the reference percolation velocity to half spreading rate. We use this dimensionless parameter following Scott and Stevenson [1989] since it should control the ratio of buoyancy effects to plate spreading effects for a given mantle viscosity. For one set of calculations we take the average mantle viscosity $\mu_0 = 10^{18}$ Pa s and for another set we take $\mu_0 = 10^{19}$ Pa s. There is no reduction in viscosity due to the presence of melt in the mantle (i.e., $\phi_0 = \infty$). The ratio of v_r to v_p is varied between 1 and 100.

For the calculations with a viscosity of 10^{19} Pa s, buoyant flow has little effect on the width of the region of crustal accretion. This is because when the viscosity is high, the plate spreading effect dominates the whole process. With $\mu_0 = 10^{18}$ Pa s the crustal accretion zone is narrowest for v_r/v_p between about 30 and 100. When this ratio is very large, there will be little melt left in the mantle to affect the flow. When the ratio is very small, melt percolates out of the mantle very slowly. Therefore lateral variations in the melt fraction do not develop under the spreading center, and the flow field is little affected by the melt. For v_r/v_p larger than about 500 we could find no

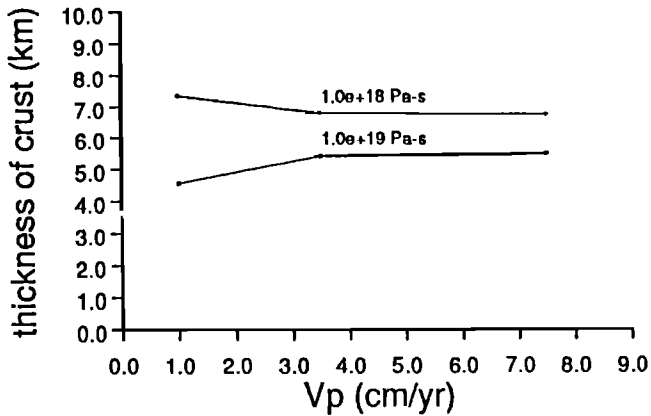


Fig. 5. Relationship between crustal thickness and spreading rate. When the viscosity of the mantle is 10^{19} Pa s, the crustal thickness is lower for small spreading rates; however, for a viscosity of 10^{18} Pa s the amount of melt produced actually increases at slow spreading rates. This may reflect an effect of thermal convection.

steady state solutions to the flow field for a viscosity of 10^{18} Pa s. Our results corroborate the results of *Scott and Stevenson* [1989], who analyzed this instability in the flow field; they attribute the instability to the interaction of the buoyancy effects of melt retention and depletion.

The effect of different spreading rates on the crustal thickness is shown in Figure 5. When the viscosity of the mantle is 10^{19} Pa s, the crustal thickness is lower for spreading rates less than about 0.03 m/yr. This is the same behavior seen in other models for generation of oceanic crust such as those of *Reid and Jackson* [1981] and *Sotin and Parmentier* [1989]. When the spreading rate is low, conductive cooling reduces mantle temperatures to a considerable depth below the spreading center. If it is too cool for melting to occur at these depths, the amount of melt produced is reduced and hence the crust is thinner.

For a viscosity of 10^{18} Pa s the amount of melt produced actually increases at slow spreading rates (Figure 5). This may reflect the effect of thermal convection. The flow patterns for the case of $\mu_0 = 10^{18}$ Pa s (Figure 5) are illustrated in Figure 6. The reference velocity is 1 m/yr, and the half-spreading rates are 0.01, 0.035, and 0.075 m/yr. The flow in the region where significant melt is retained in the mantle is clearly more focused for the slower spreading rates. The streamlines for the case with $v_p = 0.035$ m/yr are clearly closer together under the ridge than for the case with $v_p = 0.075$ m/yr. The plots of crustal thickness also reflect the greater concentration of upwelling at the slower spreading rates. The crust attains its full thickness closer to the spreading center for the slower spreading rates. These results are easy to understand because the viscous stresses related to plate separation scale with the spreading rate. Therefore the flow widens where these stresses are relatively more important. The plot of width as a function of spreading rate (Figure 4) shows these results as well.

In Figure 6 we also plot contours of total and thermal density variations relative to ρ_0 , the density at $T = T_m$, and $F = \phi = 0$ (see equation (7)). The contour interval is 20 kg/m^3 for total density variations, and the value beneath the ridge is over -75 kg/m^3 at $v_p = 0.075$ m/yr and around -55 kg/m^3 at $v_p = 0.01$ m/yr. Material is lighter and more melt remains in the matrix at fast spreading rates than at slow spreading rates. This is also

shown by shading of melt fraction on the plot of flow patterns. Note that the lateral gradient of total buoyancy from -55 kg/m^3 to -15 kg/m^3 is larger at $v_p = 0.01$ m/yr than at $v_p = 0.075$ m/yr. Upwelling is more focused at slow spreading rates; this is consistent with the plot of oceanic crustal thickness. The contour interval is 4 kg/m^3 for density variations due only to temperature variations. Thermal density variations are always positive because the temperature in the calculation region is smaller than T_m . Comparing contour plots of both total and thermal density variations shows that the latter becomes important and controls the density variation pattern far from the ridge.

Thermal density variations appear to affect the flow both within the box and through the boundaries. For the 0.01-m/yr half spreading rate the mantle below the lithosphere at the outflow boundary is moving horizontally faster than the lithosphere (the streamlines are closer together under the lithosphere than within it). Thus there is more flow coming in and going out of the box than would occur with plate-driven flow alone. Since all the material coming into the box is assigned a temperature of 1300°C , there is potentially more hot material fluxing through the melting region. For the faster spreading rates this thermally driven flow appears to be less important, and the total crustal thickness is lower than for the case with $v_p = 0.01$ m/yr. For a reference viscosity of 10^{19} Pa s, no increase in crustal thickness with decreasing spreading rate is seen. Apparently thermal convection is not important when the average mantle viscosity is this large.

In Figure 7a we show the distribution of sublithospheric melt fractions and the corresponding p wave one-way travel time delay with distance from the spreading center for two values of v_r/v_p in two melt fraction independent viscosity cases. The left side axis reflects the average amount of melt from 60 km depth up to the base of the lithosphere, and the right side axis reflects the p wave one-way travel time delay caused by melt retained in the mantle assuming there are vertical rays and linear velocity decrease as melt fraction increases [see *Sato et al.*, 1988, Figure 3].

The gravity anomaly caused by melting is composed of two terms. Since the anomaly due to depletion varies smoothly with an amplitude difference of only 2 mGal over 50 km (Figure 7b), we show the distribution of the gravity anomaly with distance from the spreading center caused by the distribution of sublithospheric melt fractions for the case with $v_r/v_p = 100$. The amplitude and wavelength of our results are similar to the residual gravity signal left after the removal of the signals due to plate cooling and topography for two areas of the East Pacific Rise at $7^\circ\text{-}9^\circ\text{S}$ analyzed by *Wang and Cochran* (submitted manuscript, 1992) and at 9.5°N analyzed by *Wilson* [1992].

In Figure 8 we illustrate the average melt fraction within the melting region from 60 km below the surface to the base of the lithosphere for cases related to melt fraction independent viscosity with $\mu_0 = 10^{18}$ Pa s and $\phi_0 = \infty$, and melt fraction dependent viscosity with $\mu_0 = 10^{19}$ Pa s and $\phi_0 = 0.02$. Two kinds of averaging methods are used, one based on the average value in an area and the other in a column beneath the ridge. For different ratios of the reference percolation velocity to the plate velocity, we see different average amounts of melt. Note in Figure 8 that over a range of values of v_r/v_p larger than 25 the average melt fraction within 50 km of the ridge is close to 2%.

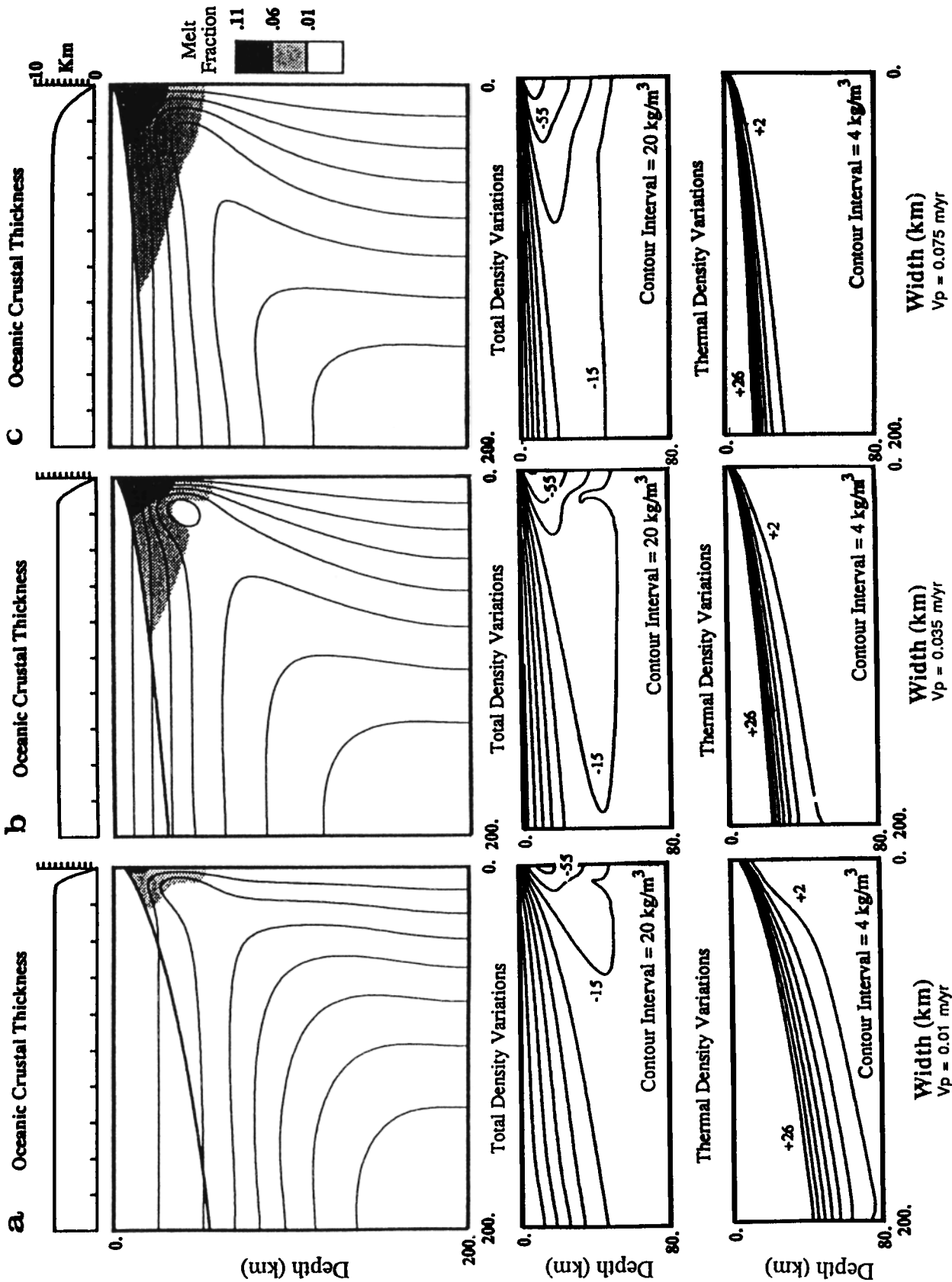


Fig. 6. Flow patterns for three calculations which define the curve in Figure 5 for the case of $\mu_0 = 10^{18}$ Pa s. The half-spreading rates are (a) 0.01, (b) 0.035, and (c) 0.075 m/yr, respectively. The flow within a few tens of kilometers of the region where significant melt is retained is clearly more focused for the slower spreading rates (Figure 6a). The plots of crustal thickness and total and thermal density variations also reflect the greater concentration of upwelling at the slower spreading rates.

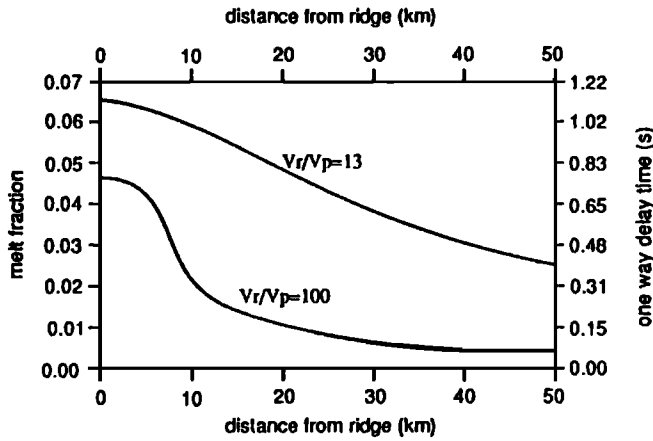


Fig. 7a. The distribution of sublithospheric melt fractions and the corresponding p wave one-way travel time delay with distance from the spreading center for two different ratios of the reference percolation velocity of Darcy flow to the plate velocity in two melt fraction independent viscosity cases. The left side axis reflects the average amount of melt from 60 km depth to the base of the lithosphere, and the right side axis reflects the p wave one-way travel time delay caused by melt retained in the mantle assuming there are vertical rays and linear velocity decrease as melt fraction increases.

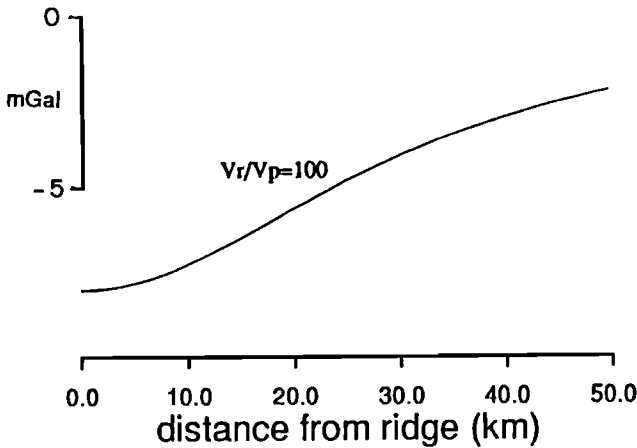


Figure 7b. The distribution of gravity anomaly with distance from the spreading center caused by the distribution of melt fraction for the case with $v_r/v_p = 100$. The amplitude and wavelength of our results are similar to the residual gravity signal left after the removal of the signals due to plate cooling and topography for two areas of the East Pacific Rise.

Viscosity Dependence on Melt Fraction

When the average mantle viscosity at shallow depths is 10^{18} Pa s, or lower, then small-scale thermal convection results in significant cooling of the mantle. The cooling causes the average mantle viscosity to increase. This larger viscosity damps the thermally driven convection. Eventually, an equilibrium temperature and associated average viscosity is reached. This self-adjustment of thermal convection is a result expected for any convecting system with a strongly temperature dependent viscosity [e.g., Tozer, 1965]. We suggest that 10^{19} Pa s is a reasonable average mantle viscosity. The viscosity cannot be much lower than this in a steady state. When the viscosity is lower, the convective flow would rapidly cool the shallow mantle. Therefore in the remaining

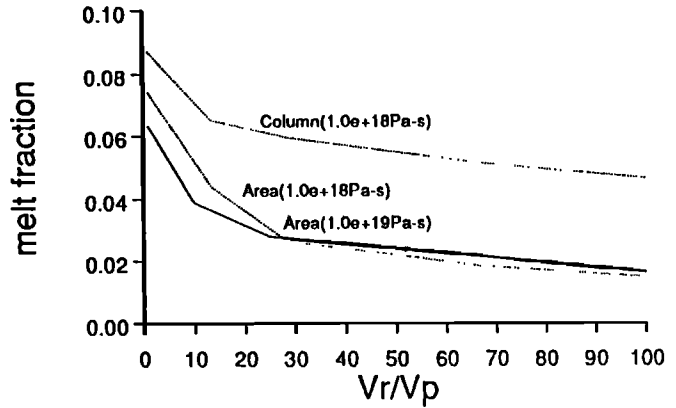


Fig. 8. Average melt fraction within the melting region from 60 km below the surface to the base of the lithosphere for the cases related to melt fraction independent viscosity with $\mu_0 = 10^{18}$ Pa s and $\phi_0 = \infty$, and melt fraction dependent viscosity with $\mu_0 = 10^{19}$ Pa s and $\phi_0 = 0.02$. "Column" indicates the average melt fraction in a vertical column beneath the ridge. "Area" refers to the average melt fraction within 50 km of the ridge. Note that for v_r/v_p larger than 25, the average melt fraction in the ridge area is close to 2%.

calculations we assume a reference viscosity of 10^{19} Pa s. The only way for there to be significant buoyancy effects on the flow is for the local viscosity to be reduced by some effect which we take to be related to the presence of melt in the mantle.

In a set of calculations presented in Figure 9 we varied the parameters ϕ_0 and v_r/v_p . The value of ϕ_0 controls the dependence of viscosity on melt fraction as given by equation (8). The smaller the value of ϕ_0 , the stronger the dependence of viscosity on melt fraction. The value of v_r/v_p controls the amount of melt that can be retained in the melting region. For a given value of plate velocity v_p the ratio is controlled by the permeability of the mantle. The numbers on the plot show the ratio of the maximum vertical velocity V_{max} to the plate velocity and reflect the width of upwelling. For example, in Figure 3e the upwelling is very narrow, and the maximum

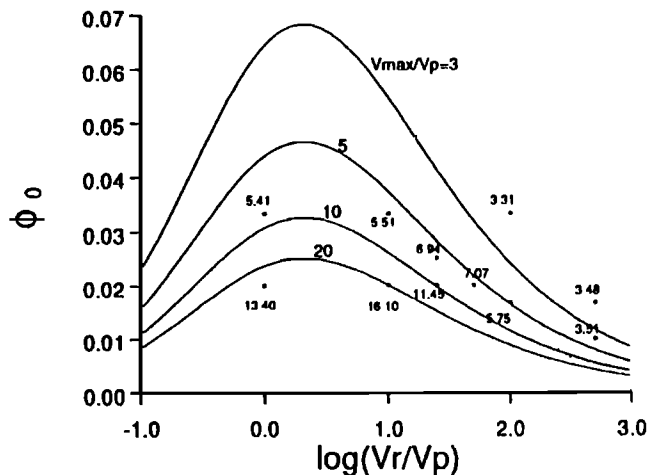


Fig. 9. Comparison between numerical and theoretical calculations of the ratio of the maximum vertical velocity V_{max} to the plate velocity for cases of melt fraction dependent viscosity. The ratios reflect how narrow the upwelling is. The reference viscosity in these calculations is 10^{19} Pa s. The value of ϕ_0 controls the dependence of viscosity on melt fraction as given by equation (7). The lines in the figure show the results of a simple analytical model described in the appendix.

vertical velocity is about 15 times the plate velocity. For Figure 3b the upwelling is not very narrow, and the maximum velocity is only 1.5 times the plate velocity.

How strong the focusing of the upwelling is in our model depends on both parameters considered. In Figure 9 we see that for a given v_r/v_p , lower values of ϕ_0 will give more concentrated upwelling. This is not surprising because for the same initial melt distribution, lower values of ϕ_0 cause lower local viscosities. For $\phi_0 = 1\%$ the viscosity is reduced by a factor of 10 for $\phi = 2.3\%$. In Figure 9 we also see that for a given ϕ_0 the focusing of melt has a peak value around $v_r/v_p = 5$. When v_r/v_p is less than 1.0, melt segregates from the mantle so slowly that large melt fraction can exist even where the upwelling velocity is small (i.e., away from the center of spreading). Thus lateral gradients in melt fraction are small. Without large lateral gradient in ϕ there can be no strong lateral variation in density or viscosity. Fast upwelling depends on these lateral variations.

For v_r/v_p greater than 1000 the situation is quite different. Melt moves so quickly, relative to the matrix, that large melt fraction cannot exist below the ridge. Buoyancy and viscosity effects that depend on melt fraction are therefore unable to affect the mantle upwelling strongly.

Reasonable values of parameters defined in equation (8) fall into a region with $\log(v_r/v_p)$ between about 0 and 5. For example, with a grain size of 0.1 mm the reference velocity v_r

= 0.0525 m/yr, and if $v_p = 0.10$ m/yr, then $\log(v_r/v_p) = -0.28$. Were the grain size 10 mm and $v_p = 0.01$ m/yr, then $\log(v_r/v_p) = 4.72$. It is numerically difficult to calculate results for very high permeability cases; fortunately, an analytical calculation may act as a guide.

The lines in Figure 9 show the results of a simple analytical model described in the appendix. The first step in the model is to calculate the melt fraction that can build up below a ridge assuming a given reference velocity. We approximate the upwelling under the ridge as being at constant velocity equal to v_p . The melt fraction at the top of the melting region is given by equation (A2). The viscosity at the top of the melting region is reduced by an amount that depends on the melt fraction and on ϕ_0 . The upwelling velocity should be large when the viscosity under the ridge is small compared to the viscosity away from the ridge. A short distance from the center of spreading the average velocity of upwelling will be lower than it is under the center. Therefore the second step is to calculate the melt fraction at the top of a melting column where the upwelling velocity has a constant value of $v_p/10$. The difference in the melt fraction at the top of the subridge column compared to the off-ridge column $\Delta\phi$ should control the difference in viscosities in the two areas. Last, we assume $V_{max}/v_p = \exp(\Delta\phi/\phi_0)$. In other words, the velocity of the upwelling is proportional to the ratio of the viscosity at the top of the off-ridge column to the viscosity at the top of the

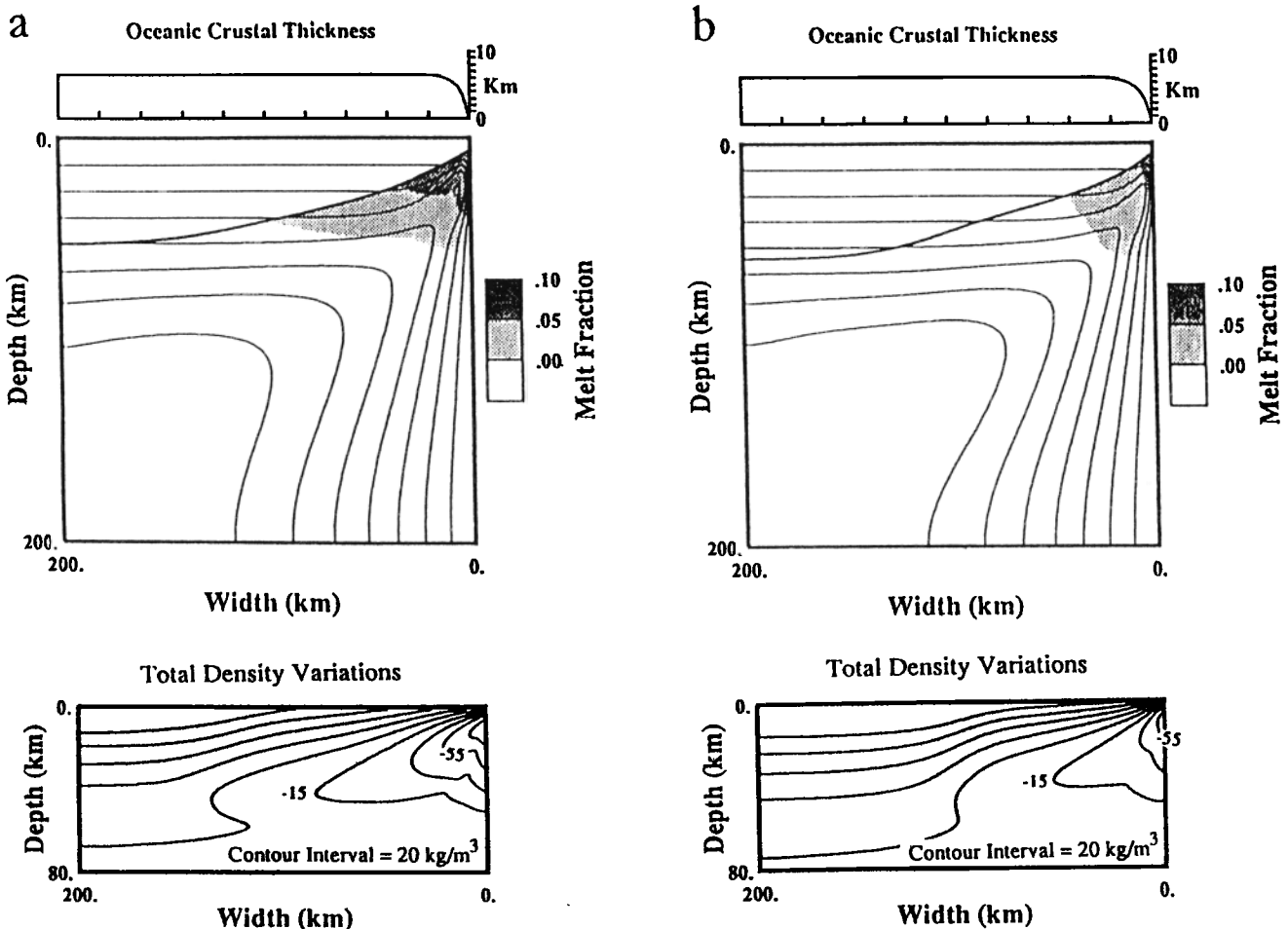


Fig. 10. Two flow patterns and the corresponding distribution of melt fraction and gravity anomaly for melt focusing under ridges with average mantle viscosity equal 10^{19} Pa s. For Figure 10a, $v_r/v_p = 10$ and $\phi_0 = 0.02$, and in Figure 10b, $v_r/v_p = 100$ and $\phi_0 = 0.0125$. The calculated values of V_{max}/v_p are 16.01 for Figure 10a and 15.44 for Figure 10b.

subridge column. Although there are several assumptions in this one-dimensional model, the theoretical results match the two-dimensional numerical calculations well within a range of parameters.

In Figure 10 we show two possible flow patterns and the corresponding distributions of melt fraction and gravity anomaly for calculations with average mantle viscosity equal 10^{19} Pa s. In Figures 10a and 10b, V_{max}/v_p are equal to 16.01 and 15.44, respectively, so they have a very similar distribution of crustal thickness shown in top of the figure. For Figure 10a we choose v_r/v_p equal 10 and $\phi_0 = 0.02$, and in Figure 10b we have $v_r/v_p = 100$ and $\phi_0 = 0.0125$. Figure 10a corresponds to a low-permeability case in which the melt fraction at a given depth is large, as are density variations shown in the bottom of the figure. Figure 10b corresponds to a relatively large permeability. Since less melt is retained in the upwelling for this case, a smaller value of ϕ_0 is needed to reduce the viscosity.

In Figures 11a and 11b there are two curves for each figure which correspond to the distributions of melt fraction and gravity anomaly for cases of Figures 10a and 10b. These two

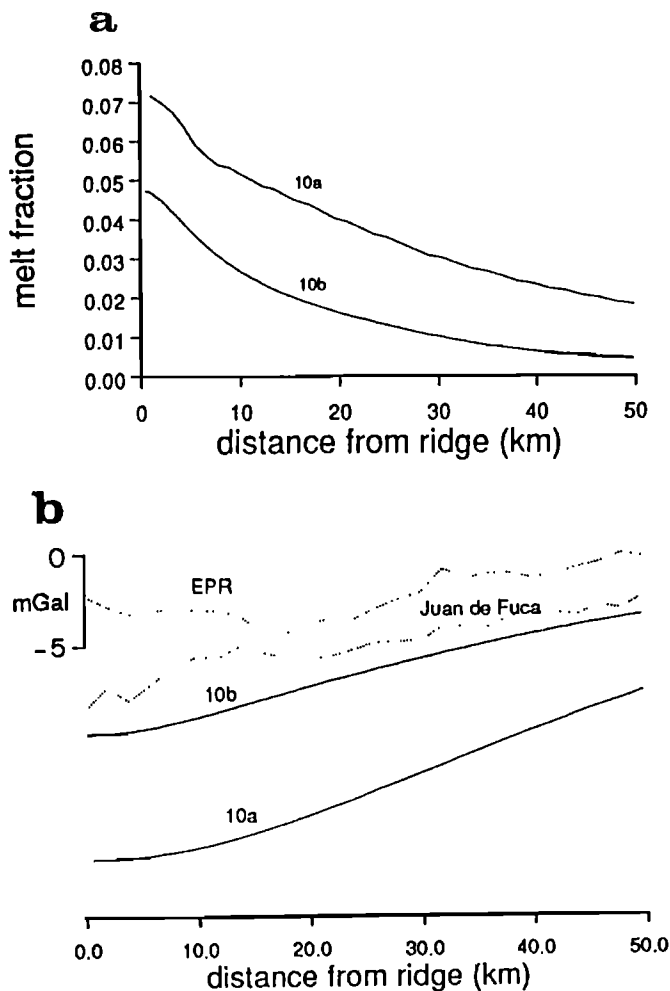


Fig. 11. In Figures 11a and 11b there are two curves which correspond to the distributions of melt fraction and gravity anomaly for the cases of Figure 10a and 10b. Residual gravity signals from the East Pacific Rise near 9.5°N and the Juan de Fuca ridge near 45°N , corrected for the effects of plate cooling and topography [Wilson, 1992], are shown as dotted lines in Figure 11b. The amplitude and wavelength of the predicted gravity anomaly and the data are consistent.

plots reflect the differences in the distribution of melt fraction and gravity anomaly due to different permeabilities. Residual gravity signals from the EPR near 9.5°N and the Juan de Fuca ridge near 45°N , corrected for the effects of plate cooling and topography [Wilson, 1992], are shown as dotted lines in Figure 11b. The amplitude and wavelength of the predicted gravity anomaly and the data are consistent.

DISCUSSION

The most important result of this work is that we have mapped out the range of parameters of permeability and viscosity over which buoyancy effects could result in very narrow subridge mantle upwelling. We have shown how the distribution and amount of melt in the mantle depend on permeability and the relation between melt fraction and viscosity. Our results also have implications about the relation between oceanic crustal thickness and spreading rate, and about the average shallow viscosity. All these results can be used to interpret observed data.

Our results on thermal convection below ridges may have implications for the effect of regional variations in mantle temperature on crustal thickness. Seismic observations indicate that the average thickness of oceanic crust is not a strong function of spreading rate, although there appears to be more scatter in crustal thickness at slow spreading rates [White *et al.*, 1992; Chen, 1992; Mutter and Mutter, submitted manuscript, 1992]. Our calculations for an average viscosity $\mu_0 = 10^{19}$ Pa s show a weak dependence of crustal thickness on spreading rate, with thickness decreasing as the spreading rate is reduced. This is similar to the results of Sotin and Parmentier [1989], who consider a model in which subridge mantle flow is driven by viscous stresses as well as thermal- and depletion-related buoyancy. We find a different result for lower mantle viscosities. For an average viscosity of 10^{18} Pa s the amount of melt produced actually increases with decreasing spreading rate as shown in Figure 5. We believe this phenomenon is explained by thermal convection. For faster spreading rates, thermal convection has a smaller effect on the average amount of melt produced.

A region of mantle at higher than the average temperature should cause the total amount of melt produced by upwelling under a ridge to be larger for two reasons. The higher temperature should allow melting to begin deeper in the mantle and cause the degree of melting at shallow depth to be larger. The increased temperature should also reduce the viscosity of the mantle and may lead to rapid thermal convection. This convection causes a greater volume of mantle to flux through the melting region, thus increasing the amount of melt produced per unit of plate separation. Our results indicate that the effect of thermal convection on the amount of melt produced is more important at slow spreading rates than at fast spreading rates. Thermal convection essentially amplifies the effect of regional mantle temperature variations in terms of crustal thickness. Since this amplification is more important at slow spreading rates, this may explain why the range of crustal thickness is wider for slow spreading ridges than for fast spreading ridges. All previous compilations of oceanic crustal thickness versus spreading rate are based on data collected at different places where mantle temperature could be very different. It would be helpful to use data collected in regions where the spreading rate is known to vary in time, such as close to the Chile Rise.

Our results on the effect of thermal convection may also have implications for the process of melting during the formation of passive margins. Basalt sequences up to 20 km thick have been imaged seismically along some passive margins [Mutter *et al.*, 1988; Zehnder *et al.*, 1990; Hopper *et al.*, 1992]. These sequences are emplaced in time intervals as short as a few million years or less [Mutter *et al.*, 1988]. Many authors have noted that these "volcanic passive margins" are located close to major mantle plumes, and they infer that the plumes may have caused a large area of mantle below the region of continental breakup to be very hot [Vink, 1984; White and McKenzie, 1989; Griffith and Campbell, 1990]. Hot mantle should melt more than normal mantle as the continents extend and seafloor spreading begins. The effects of small-scale thermal convection could explain the short time interval over which these sequences form. If the mantle temperature below a nascent spreading center were 200°C hotter than normal, then the viscosity there would be about 2 orders of magnitude lower than normal. Thermal convection would then cause very rapid flow of a large volume of mantle through the melting region, and so quantities of melt would be produced. The convection would rapidly cool the mantle, the viscosity would increase, and thermal convection would slow. This transient phase of rapid convection might be over in a few million years, and the amount of melting would become more like that for normal ridges.

We suggest that the topographic highs at fast spreading ridges are supported by the flow stress on the base of the lithosphere caused by melt rich buoyant upwelling under a ridge. This has also been suggested by Madsen *et al.* [1984] and Wilson [1992]. Our calculations show that the mantle permeability cannot be too high and still result in the several percent melt retention in the subridge mantle that could support the axial topographic high. We roughly estimate that the reference velocity for Darcy flow cannot exceed 10 m/yr and still explain the topography at the EPR. At slow spreading ridges the upward stress related to buoyant flow must be less than the stresses related to necking the thick cold lithosphere [Tapponnier and Francheteau, 1978; Lin and Parmentier, 1989; Chen and Morgan, 1990], and thus no axial high results.

The amount of focusing of mantle upwelling due to all buoyancy terms depends on the viscosity of the mantle. The lower the viscosity is, the more focused the upwelling. However, if the shallow average mantle viscosity is much less than 10^{19} Pa s, then small-scale thermal convection should lead to rapid cooling of the mantle. Thus such low average viscosities can only exist as transients. We conclude that local viscosity reduction related to partial melting is necessary to obtain very narrow, buoyancy-driven upwelling consistent with observations. The required strength of the functional dependence of local viscosity on melt fraction is determined by the mantle permeability and reference viscosity. In Figure 9 we have shown their relations through a series of numerical calculations with average viscosity $\mu_0 = 10^{19}$ Pa s. If the permeability is large, then the local viscosity must be a strong function of melt fraction. Because the numerical calculations become more difficult when the permeability is large or viscosity is small, we developed a simple theoretical method to predict the trend. Although there are several assumptions in this one-dimensional model, numerical calculations and analytical results match well within a range of parameters. Our numerical results and theoretical analysis suggest that upwelling can be very focused under ridges for a wide range of

mantle permeabilities as long as the local viscosity is a strong function of melt fraction.

For the cases with strong lowering of the viscosity where the melt fraction is largest, the width of the fast upwelling is much narrower than the region of melt delivery to the surface. This is a result of the lateral transport of melt with the diverging mantle flow below the ridge which is analogous to stagnation point flow. If veins or dikes were to form in the region of high melt fraction and fast upwelling, then most of the melt would be delivered extremely close to the spreading center for the melt fraction dependent cases. For example, if we calculated the melt delivery to the crust at a depth of 2 km below the lithosphere for the case shown in Figure 10b, then most of the melt would get to the crust within a kilometer of the spreading axis.

The distribution of melt fraction below ridges is another very interesting question. Existing geochemical and geophysical data give no clear picture of the average melt fraction below ridges. In Figure 8 we show the average interconnected melt fraction within 50 km of the ridge for a range of cases which all gave very narrow mantle upwelling below the ridge. With the ratio of the reference velocity to the half spreading rate v_r/v_p varying from about 25 to 100, the average melt fraction is close to 2%. The average melt fraction increases rapidly when v_r/v_p is less than 25. Note that the calculations are done with $\mu_0 = 10^{19}$ Pa s and for the case of melt fraction dependent viscosity. We infer that the melt fraction retained in the mantle is relatively insensitive to the mantle permeability, above a certain value, because most of the melt is advectively transported to the surface. This occurs because most of the melt is produced in the narrow area of rapid upwelling. Only when the permeability is so low that the melt flow is much slower than the plate flow do we see significant retention of melt in the mantle.

In our calculations there are three important model parameters and three model predictions. The three parameters are reference mantle viscosity, permeability, and spreading rate. The three predictions, which can be measured at spreading centers, are the distribution of melt in the subridge mantle, the width over which melt is delivered to the crust, and the predicted crustal thickness. Therefore the relationships between these model parameters and predictions can be tested by observation. It should be remembered that our model is based on some very uncertain assumptions, particularly the relations between permeability and viscosity on melt fraction. We have assumed simple functional relations between these quantities and calculated results for a wide range of parameters. Clearly, further physical and chemical experiments on the properties of mantle materials are needed to clarify these relations.

APPENDIX: ANALYTIC TREATMENT OF FLOW CONCENTRATION

Consider the viscosity of the shallow mantle to be dependent on temperature and melt fraction as expressed in equation (7). The reference viscosity at the maximum temperature, μ_0 , is assumed to be 10^{19} Pa s. To obtain a concentrated upwelling under a spreading center requires that the viscosity be reduced by the presence of melt to a value of μ_{\min} . If the maximum melt fraction present in the upwelling is ϕ_{\max} , then

$$\mu_{\min}/\mu_0 = \exp(-\phi_{\max}/\phi_0) \quad (A1)$$

where ϕ_0 is a constant in equation (7).

Assuming that without any viscosity reduction due to the presence of melt the velocity in the upwelling is equal to the plate spreading velocity v_p , we can estimate the maximum melt fraction at the top of the upwelling. For a reference Darcy velocity v_r and a maximum degree of melting at the top of the upwelling of F_{max} [see Buck and Su, 1989; Scott and Stevenson, 1989],

$$\phi_{max} = [(v_p/2v_r)^2 + (v_p/v_r)F_{max}]^{1/2} - v_p/2v_r \quad (A2)$$

Assume that μ_{min} is a critical value of the viscosity that allows melt buoyancy effects to produce a concentrated upwelling. For given physical parameters μ_0 , v_p , v_r , and F_{max} , the parameter ϕ_0 must be small enough for the viscosity to be lowered to μ_{min} . This can happen when

$$\phi_0 = \phi_{max} / \ln(\mu_0/\mu_{min}) \quad (A3)$$

Combining equations (A2) and (A3), we can calculate the values of ϕ_0 required to reduce the viscosity in the upwelling by a given amount. The results for a range of values of v_p/v_r are shown in Figure 9.

Acknowledgments. We thank Marc Spiegelman, John Mutter, Jim Cochran, and Xuejin Wang for helpful discussions and comments on the paper. Thanks also to Doug Wilson, an anonymous reviewer, and an associate editor for careful and constructive reviews of the manuscript. Support for this work came from OCE89-12004 and OCE 92-00945. This is Lamont-Doherty Earth Observatory contribution 5304.

REFERENCE

- Ahem, J. L., and D. L. Turcotte, Magma migration beneath an ocean ridge, *Earth Planet. Sci. Lett.*, **45**, 115-122, 1979.
- Batchelor, G. K., *An Introduction to Fluid Dynamics*, Cambridge University Press, New York, 1967.
- Borch, R. S., and H. W. Green, Experimental investigation of the rheology and structure of partially molten ilmenite deformed under upper mantle pressures and temperatures (abstract), *Eos, Trans. AGU*, **71**, 629, 1990.
- Buck, W. R., and E. M. Parmentier, Convection beneath young oceanic lithosphere: implications for thermal structure and gravity, *J. Geophys. Res.*, **91**, 1,961-1,974, 1986.
- Buck, W. R., and W. Su, Focused mantle upwelling below mid-ocean ridges due to feedback between viscosity and melting, *Geophys. Res. Lett.*, **16**, 641-644, 1989.
- Cheadle, M. J., Properties of texturally equilibrated two-phase aggregates, Ph.D. thesis, 156 pp., Univ. of Cambridge, Cambridge, England, 1989.
- Chen, Y. J., Oceanic crustal thickness versus spreading rate, *Geophys. Res. Lett.*, **19**, 753-756, 1992.
- Chen, Y. J., and W. J. Morgan, A nonlinear rheology model for mid-ocean ridge axis topography, *J. Geophys. Res.*, **95**, 17,583-17,604, 1990.
- Cooper, R. F., and D. L. Kohlstedt, Solution-precipitation enhanced diffusional creep of partial molten olivine-basalt aggregates during hot-pressing, *Tectonophysics*, **107**, 207-233, 1984.
- Cooper, R. F., and D. L. Kohlstedt, Rheology and structure of olivine-basalt partial melts, *J. Geophys. Res.*, **91**, 9315-9323, 1986.
- Detrick, R. S., P. Buhl, E. Vera, J. Mutter, J. Orcutt, J. Madsen, T. Brocher, Multichannel seismic imaging of a crustal magma chamber along the East Pacific Rise, *Nature*, **326**, 35-41, 1987.
- Forsyth, D. W., Seismological constraints on partial melting beneath the East Pacific Rise (abstract), *Eos, Trans. AGU*, **73**(14), Spring Meeting Suppl., 290, 1992.
- Griffith, R. W., and I. H. Campbell, Stirring and structure in mantle starting plumes, *Earth Planet. Sci. Lett.*, **99**, 66-78, 1990.
- Hopper, J. R., J. C. Mutter, R. L. Larson, C. Z. Mutter, and the Northwest Australia Study Group, Magmatism and rift margin evolution: Evidence from Northwest Australia, *Geology*, pp853-858, 1992.
- Klein, E. M., and C. H. Langmuir, Global correlations of ocean ridge basalt chemistry with axial depth and crustal thickness, *J. Geophys. Res.*, **92**, 8089-8115, 1987.
- Kushiro, I., Viscosity of partial melts in the upper mantle, *J. Geophys. Res.*, **91**, 9343-9350, 1986.
- Lax, P. D., and R. D. Richtmyer, Survey of the stability of linear finite difference equations, *Commun. Pure Appl. Math.*, **9**, 267-293, 1956.
- Lin, J., and E. M. Parmentier, Mechanisms of lithospheric extension at mid-ocean ridges, *Geophys. J.*, **96**, 1-22, 1989.
- Madsen, J. A., D. W. Forsyth, and R. S. Detrick, A new isostatic model for the East Pacific Rise crest, *J. Geophys. Res.*, **89**, 9,997-10,015, 1984.
- McKenzie, D. P., The generation and compaction of partial melts, *J. Petrol.*, **25**, 713-765, 1984.
- McKenzie, D., and M. J. Bickle, The volume and composition of melt generated by extension of the lithosphere, *J. Petrol.*, **29**, 625-679, 1988.
- Mutter, J. C., W. R. Buck, and C. M. Zehnder, Convective partial melting, I, A model for the formation of thick basaltic sequences during the initiation of spreading, *J. Geophys. Res.*, **93**, 1031-1048, 1988.
- Parmentier, E. M., Studies of thermal convection with application to convection in the Earth's mantle, Ph.D. thesis, Cornell Univ., Ithaca, N. Y., 1975.
- Phipps Morgan, J., Melt migration beneath mid-ocean spreading centers, *Geophys. Res. Lett.*, **14**, 1238-1241, 1987.
- Plank, T., and C. H. Langmuir, Effects of the melting regime on the composition of the oceanic crust, *J. Geophys. Res.*, **97**, 19,749-19,770, 1992.
- Rabinowicz, M., A. Nicolas, and J. L. Vigneresse, A rolling mill effect in asthenospheric beneath oceanic spreading centers, *Earth Planet. Sci. Lett.*, **67**, 97-108, 1984.
- Reid, I., and H. R. Jackson, Oceanic spreading rate and crustal thickness, *Mar. Geophys. Res.*, **5**, 165-172, 1981.
- Ribe, N. M., The deformation and compaction of partially molten zones, *Geophys. J. R. Astron. Soc.*, **83**, 487-501, 1985.
- Salters, V. J. M., and S. R. Hart, The hafnium paradox and the role of garnet in the source of mid-ocean-ridge basalts, *Nature*, **342**, 420-422, 1989.
- Sato, H., I. S. Sacks, T. Murase, and C. M. Scarfe, Thermal structure of the low velocity zone derived from laboratory and seismic investigations, *Geophys. Res. Lett.*, **15**, 1227-1230, 1988.
- Scott, D. R., and D. J. Stevenson, A self-consistent model of melting, magma migration, and buoyancy-driven circulation beneath a mid-ocean ridge, *J. Geophys. Res.*, **94**, 2973-2988, 1989.
- Sotin, C., and E. M. Parmentier, Dynamical consequences of compositional and thermal density stratification beneath spreading centers, *Geophys. Res. Lett.*, **16**, 835-838, 1989.
- Sparks, D. W., and E. M. Parmentier, Melt extraction from the mantle beneath spreading centers, *Earth Planet. Sci. Lett.*, **105**, 368-377, 1991.
- Spiegelman, M., Flow in deformable porous media, Part I, simple analysis, *J. Fluid Mech.*, **247**, 17-38, 1993a.
- Spiegelman, M., Flow in deformable porous media, Part II, numerical analysis-the relationship between shock waves and solitary waves, *J. Fluid Mech.*, **247**, 39-63, 1993b.
- Spiegelman, M., and D. P. McKenzie, Simple 2-D models for melt extraction at mid-ocean ridges and island arcs, *Earth Planet. Sci. Lett.*, **83**, 137-152, 1987.
- Tapponnier, P., and J. Francheteau, Necking of the lithosphere and the mechanics of slowly accreting plate boundaries, *J. Geophys. Res.*, **83**, 3955-3870, 1978.
- Torrance, K. E., Comparison of finite difference computations of natural convection, *J. Res. Natl. Bur. Stand.*, **72**, Sect. B, 281-301, 1968.
- Tozer, D. C., Heat transfer and convection currents, *Philos. Trans. R. Soc. London Ser. A*, **258**, 252-271, 1965.
- Vink, G. E., A hotspot model for Iceland and Voring plateau, *J. Geophys. Res.*, **89**, 9,949-9,959, 1984.
- Waff, H. S., and J. R. Bulau, Equilibrium fluid distribution in an ultramafic partial melt under hydrostatic stress conditions, *J. Geophys. Res.*, **84**, 6109-6114, 1979.
- Waff, H. S., and U. H. Faul, Effect of crystalline anisotropy on fluid distribution in ultramafic partial melts, *J. Geophys. Res.*, **97**, 9,003-9,014, 1992.

- Weertman, J., and J. R. Weertman, High temperature creep of rock and mantle viscosity, *Annu. Rev. Earth Planet. Sci.*, **3**, 293-315, 1975.
- White, R. S., and D. McKenzie, Magmatism at rift zones: The generation of volcanic continental margins and flood basalts, *J. Geophys. Res.*, **94**, 7,685-7,730, 1989.
- White, R. S., D. McKenzie, and R. K. O'Nions, Oceanic crustal thickness from seismic measurements and rare earth element inversions, *J. Geophys. Res.*, **97**, 19,683-19,715, 1992.
- Wilson, D. S., Focused mantle upwelling beneath mid-ocean ridges: Evidence from seamount formation and isostatic compensation of topography, *Earth Planet. Sci. Lett.*, **113**, 41-55, 1992.
- Zehnder, C. M., J. C. Mutter, and P. Buhl, Deep seismic and geochemical constraints on the nature of magmatism during breakup of the North Atlantic, *Tectonophysics*, **173**, 545-565, 1990.
-
- W. R. Buck and W. Su, Multichannel Seismics Group, Lamont-Doherty Earth Observatory, Palisades, NY 10964.

(Received August 3, 1992;
revised March 29, 1993;
accepted April 12, 1993.)